bioRxiv preprint doi: https://doi.org/10.1101/2020.05.20.106328; this version posted May 21, 2020. The copyright holder for this preprint (which was not certified by peer review) is the author/funder, who has granted bioRxiv a license to display the preprint in perpetuity. It is made available under aCC-BY 4.0 International license.

1 **Wnt16 Elicits a Protective Effect Against Fractures and Supports Bone Repair in**
2 **Zebrafish**
3
4 Running title: Wnt16 in zebrafish fracture
5
6 Lucy M. McGowan[1], Erika Kague[1], Alistair Vorster[1], Elis Newham[1], Stephen Cross[2], Chrissy
7 L. Hammond*[1]
8
9 1. School of Physiology, Pharmacology and Neuroscience, University of Bristol, Bristol,
10 United Kingdom, BS8 1TD.
11 2. Wolfson Bioimaging Facility, University of Bristol, Bristol, United Kingdom, BS8 1TD.
12 *Correspondence: chrissy.hammond@bristol.ac.uk
13
14 **Summary**
15
16 Bone homeostasis is a dynamic, multicellular process which is required throughout life to
17 maintain bone integrity, prevent fracture and respond to skeletal damage. *WNT16* has been
18 linked to bone fragility and osteoporosis in humans, as well as functional haematopoiesis of
19 leukocytes *in vivo*, but the mechanisms by which it promotes bone health and repair are not
20 fully understood. We used CRISPR-Cas9 to generate mutant zebrafish lacking Wnt16
21 (*wnt16*$^{-/-}$) to study its effect on bone dynamically. *wnt16* mutants displayed variable tissue
22 mineral density and were susceptible to spontaneous fractures and the accumulation of
23 bone calluses at an early age. Fractures were induced in the lepidotrichia of the caudal fins
24 of *wnt16*$^{-/-}$ and wild type (WT) zebrafish; this model was used to probe the mechanisms by
25 which Wnt16 regulates skeletal and immune cell-dynamics *in vivo*. *wnt16* mutants repaired
26 fractures more slowly compared to WT zebrafish. Osteoblast cell number was reduced at the
27 fracture site 4 days post-injury in *wnt16* mutants, coinciding with prolonged activation of the
28 canonical Wnt signalling pathway. Surprisingly, we found no evidence that the recruitment of
29 innate immune cells to fractures was altered in *wnt16* mutants. This study highlights
30 zebrafish as an emerging model for functionally validating osteoporosis-associated genes
31 and investigating fracture repair dynamically *in vivo*. Using this model, we demonstrate that
32 Wnt16 protects against fracture and is likely to support bone repair by attenuating the
33 activation of the canonical Wnt signalling pathway to facilitate osteoblast recruitment and
34 bone matrix deposition.
35
36 Key words: Wnt16, skeletal, fracture, zebrafish, immune cells, osteoblasts, osteoporosis

bioRxiv preprint doi: https://doi.org/10.1101/2020.05.20.106328; this version posted May 21, 2020. The copyright holder for this preprint (which was not certified by peer review) is the author/funder, who has granted bioRxiv a license to display the preprint in perpetuity. It is made available under aCC-BY 4.0 International license.

37

38 **Introduction**

39

40 The maintenance of skeletal health is central to many essential processes in the body; in
41 addition to facilitating movement and protecting vital organs, bones regulate mineral
42 reserves, haematopoiesis and influence systemic hormone levels [1]. Skeletal homeostasis
43 is maintained by numerous cell types such as chondrocytes, osteoblasts, osteocytes,
44 osteoclasts and innate immune cells [2, 3]. These cell types act in concert to maintain an
45 optimal balance between bone deposition and bone resorption under steady state conditions
46 and respond to acute skeletal damage such as fracture [4, 5]. Osteoporosis occurs when
47 bone deposition is reduced in relation to bone resorption, resulting in low bone mineral
48 density (BMD) and loss of bone integrity [3]. Poor bone quality and low BMD is a strong
49 predictor of fracture risk [6]. Currently, an estimated 3.5 million people in the UK suffer with
50 osteoporosis, resulting in over half a million fractures per year [7]. Fragility fractures cause
51 extensive morbidity and pose a high socioeconomic burden; as the ageing population
52 increases, the treatment costs associated with osteoporotic bone fractures are set to rise by
53 30% in the next decade. Hence, there is an urgent unmet demand to understand the
54 underlying causes of osteoporosis, identify novel targets for therapeutic intervention and
55 promote optimal bone repair post-fracture.

56

57 Wnt signalling pathways are highly conserved, central regulators of skeletal development
58 and homeostasis which act on bone throughout the lifetime of vertebrate organisms [8].
59 Canonical Wnt pathway activation in cells leads to the stabilisation of β-catenin and
60 activation of transcription factors, whereas the calcium-dependent and planar cell polarity
61 non-canonical Wnt signalling pathways regulate intracellular calcium levels and Jun N-
62 terminal kinase (JNK) activity, respectively [9]. Wnt ligands are a family of secreted
63 glycoproteins which influence cell stemness, proliferation, differentiation and migration via
64 Wnt signalling pathways [10]. WNT16 is one such ligand which can influence the activity of
65 canonical and non-canonical Wnt pathways [11, 12]. Recently, WNT16 has emerged as a
66 potential regulator of cortical bone thickness and bone mineral density, with mutations in
67 *WNT16* being linked to osteoporosis susceptibility in human genome wide association
68 studies (GWAS) [13-15]. Furthermore, a meta-analysis of GWAS in women aged 20-45
69 years also associated *WNT16* with lumbar-spine BMD, indicating that *WNT16* may influence
70 BMD throughout life, not only in post-menopausal populations [16].

71

72 Current experimental evidence highlights WNT16 as potential regulator of bone homeostasis
73 and repair, as well as immune cell development. Knockout of *Wnt16* in mice has been

bioRxiv preprint doi: https://doi.org/10.1101/2020.05.20.106328; this version posted May 21, 2020. The copyright holder for this preprint (which was not certified by peer review) is the author/funder, who has granted bioRxiv a license to display the preprint in perpetuity. It is made available under aCC-BY 4.0 International license.

74 shown to lead to decreased cortical bone thickness and up to a 61% decrease in femur and
75 tibia bone strength compared to wild type littermates in three-point bending tests [17]. Whilst,
76 loss of *Wnt16* in mice decreases bone strength, overexpression of *Wnt16* in osteoblasts
77 (under the *Col1a1* promoter) leads to increased bone formation [18, 19]. However, one study
78 showed that *Wnt16* overexpression in osteoblasts could not counter glucocorticoid-induced
79 osteoporosis and bone loss, suggesting that other factors play a role [19]. One possible
80 explanation could include interactions with the immune system. Glucocorticoid treatment in
81 zebrafish has been demonstrated to suppress the innate immune system and osteoblast
82 activity leading to decreased bone synthesis [20]. It has also been shown that morpholino-
83 mediated knockdown of *wnt16* in zebrafish embryos results in impaired haematopoiesis and
84 loss of thymic T lymphocytes at 4 days post-fertilisation (dpf) [21]. Embryonic knockdown
85 experiments demonstrated that somatic *wnt16* expression is required for the upregulation of
86 notch ligands and subsequent expression of the haematopoietic stem cell (HSC) marker
87 *cd41*, which is needed for proper immune cell differentiation [21]. Despite its proposed role
88 in early HSC development, the relationship between Wnt16 and the immune system has not
89 been explored further in adult tissues or in stable mutant lines. Moreover, there is increasing
90 interest in the interplay between immune cells and bone; osteoclasts and macrophages are
91 derived from a common myeloid progenitor cell population and it is thought that
92 macrophages can differentiate directly into osteoclasts in response to environmental
93 molecular stimuli [22]. The rapid but tightly regulated recruitment of innate immune cells is
94 also required for optimal bone repair post-fracture [23, 24]. WNT16 has been linked to bone
95 maintenance, fracture susceptibility and leukocyte differentiation. However, functional
96 studies to elucidate the role of WNT16 in these dynamic processes are still required.
97
98 Zebrafish (*Danio rerio*) serve as excellent models for studying both the musculoskeletal
99 system and innate immunity. Approximately 85% of human disease-related genes have an
100 ortholog in zebrafish [25]; as a result, many of the developmental processes, cell types and
101 immune cell populations contributing to bone maintenance in humans are strongly
102 conserved in zebrafish [26, 27]. Crucially, transparent zebrafish fin tissue provides optical
103 clarity for high-quality, dynamic live imaging of adult bone tissue and injury repair *in vivo*
104 [28]. Recently, the crushing of zebrafish caudal fin ray bones (lepidotrichia) was established
105 as a model for studying fracture repair *in vivo* [29]. Therefore, we used CRISPR/Cas9
106 technology to generate a stable *wnt16*$^{-/-}$ mutant line of zebrafish to investigate how loss of
107 functional *wnt16* would affect bone maintenance, fracture repair and innate leukocyte
108 function. We demonstrate that lack of Wnt16 in zebrafish leads to variable tissue mineral
109 density in the fins and increased frequency of spontaneous fractures of caudal lepidotrichia
110 in early adulthood. We employed an induced fracture model, to further characterise key

bioRxiv preprint doi: https://doi.org/10.1101/2020.05.20.106328; this version posted May 21, 2020. The copyright holder for this preprint (which was not certified by peer review) is the author/funder, who has granted bioRxiv a license to display the preprint in perpetuity. It is made available under aCC-BY 4.0 International license.

111 immunological and osteological events underpinning bone repair in zebrafish. We show that
112 *wnt16*$^{-/-}$ zebrafish repair bone more slowly compared to wild type (WT) zebrafish. Impaired
113 fracture healing in *wnt16*$^{-/-}$ zebrafish coincided with higher levels of canonical Wnt activation
114 and delayed osteoblast recruitment. Surprisingly, the recruitment of innate immune cells
115 (neutrophils and macrophages) was unaffected by loss of Wnt16 post-fracture. We found no
116 measurable difference in overall osteoclast activity (tartrate-resistant acid phosphatase
117 (TRAP) staining) but observed more distinct, concentrated areas of TRAP labelling in *wnt16*
118 mutant fractures. Taken together, our data suggests that Wnt16 promotes optimal bone
119 repair post-fracture by regulating osteoblast activity and bone matrix synthesis via the
120 regulation of canonical Wnt activity. This highlights the modulation of the canonical Wnt
121 pathway and Wnt16 as potential osteo-anabolic candidates for further exploration in
122 osteoporosis therapy development. Our data also further promotes zebrafish as a novel
123 model for the dynamic study of fracture repair *in vivo* and rapid validation of human
124 osteoporosis-associated genes.
125
126 **Materials and Methods**
127
128 *Transgenic zebrafish lines and animal husbandry*
129
130 All zebrafish were maintained at the University of Bristol's Animal Scientific Unit as
131 previously described [30, 31]. Experiments were approved by local ethical committee (the
132 Animal Welfare and Ethical Review body for University of Bristol) and performed under a UK
133 Home Office project license. Transgenics used have been previously described (Table 1).
134
135 Table 1. Transgenic lines as listed on zfin.org and abbreviations used in text.

Line Name and Reference	Abbreviation	Description
Tg*(7xTCF-Xla:Siam:nlsGFP)* [32]	Wnt:GFP	Canonical Wnt activity
osx-nls:eGFP [33]	*osx*:GFP	Osteoblasts
Tg(col2a1aBAC:mCherry) [34]	*col2a1*:mCherry	Chondrocytes
Tg(mpeg1:mCherry) [35]	*mpeg1*:mCherry	Macrophages
Tg(ET30:lyzC:DsRed) [36]	*lyzC*:DsRed	Neutrophils

136
137 *wnt16 CRISPR mutant zebrafish*
138
139 gRNAs were designed targeting exon 2 of *wnt16. g*RNAs were incubated with Cas9 protein
140 (Thermo Fisher, B25641) prior to injections, performed at 1 cell stage eggs, as
141 CRISPR/Cas9 mutagenesis was used to generate G0 mosaic zebrafish carrying indel

bioRxiv preprint doi: https://doi.org/10.1101/2020.05.20.106328; this version posted May 21, 2020. The copyright holder for this preprint (which was not certified by peer review) is the author/funder, who has granted bioRxiv a license to display the preprint in perpetuity. It is made available under aCC-BY 4.0 International license.

mutations in exon 2 of *wnt16* as previously described in Brunt *et al.,* [37]. G0s were raised to 3 months and crossed to wild type fish (TL/EKK strain) to generate heterozygous G1 embryos with a variety of *wnt16* mutant alleles. DNA was extracted from G1s, followed by PCR and cloning using TOPO-TA sequencing kit (Thermo Fisher), followed by sequencing. Two alleles were selected: $wnt16^{bi667}$ (165 bp insertion, $wnt16^{a1-/-}$) and $wnt16^{bi451}$ (72 bp insertion, $wnt16^{a2-/-}$), (Supplementary Figure S1 A). Both alleles lead to a premature stop codon compromising over 85% of the protein, likely resulting in nonsense mediated decay, therefore predicted to be null mutants (Supplementary Figure S1 B). Heterozygous $wnt16^{+/-}$ fish were incrossed to generate stable homozygous ($wnt16^{-/-}$) mutants which were used in experiments.

Genotyping

Fish were genotyped by clipping the dorsal fin and placing the tissue in base solution (25 mM NaOH, 0.2 mM EDTA). Samples were heated to 98°C for 30 minutes and cooled to 4°C before neutralising with 40 mM Tris-HCl (pH 5.0). PCR was performed using EmeraldAmp® GT PCR Master Mix and *wnt16* F- TTTTCCTCGGGCCTGGTTAT; R-GCCCTCTTTAACGCTCGGTA primers. Gel electrophoresis was performed using the PCR product from each sample (1.5% agarose in TAE + 1:10 000 SYBR Safe (Invitrogen)). Genotype was determined based on band separation due to variation in amplicon length: wild type = 216 bp, $wnt16^{a1-/-}$ = 381 bp, $wnt16^{a2-/-}$ = 288 bp (Supplementary Figure S1 C).

Fracture induction

Young adult fish (6 months old) anaesthetised using MS222 (Sigma-Aldrich) and moved to a plastic dish for imaging. Lepidotrichia within the caudal fins were imaged prior to injury (see below). Fractures were induced by pressing on an individual segment of bone in the caudal fin lepidotrichia with a blunt-ended glass capillary tube. Fractures were induced proximal to the body of the fish, prior to the first bifurcation in the ray. Fish were recovered and reimaged at various time points post-injury.

Imaging of fractures

Fish were housed individually and placed under anaesthetic at time points of interest post-fracture. Fractures were imaged in the dark using a DFC700T camera mounted to a MZ10F

bioRxiv preprint doi: https://doi.org/10.1101/2020.05.20.106328; this version posted May 21, 2020. The copyright holder for this preprint (which was not certified by peer review) is the author/funder, who has granted bioRxiv a license to display the preprint in perpetuity. It is made available under aCC-BY 4.0 International license.

177 Stereomicroscope (Leica microsystems) before fish were revived immediately in fresh
178 system water. Images were acquired using LAS X software 3.7.0 (Leica microsystems).
179
180 *Live staining of bone*
181
182 To visualise bone repair in live zebrafish, various combinations of Alizarin Red stain (ARS)
183 and calcein green staining were used. ARS was composed of 74 μM Alizarin Powder
184 (Sigma-Aldrich) and 5 mM HEPES dissolved in Danieau's solution [38]. Calcein green stain
185 was composed of 40 μM calcein powder (Sigma-Aldrich) dissolved in Danieau's solution (pH
186 8) [39]. Live fish were immersed in either ARS or calcein green for one hour, then immersed
187 in fresh system water for 15 minutes prior to imaging to clear excess stain.
188
189 *Whole-mount fin immunohistochemistry*
190
191 Whole fins were amputated and fixed in 4% paraformaldehyde overnight at 4°C. Fins were
192 dehydrated in a series of increasing concentrations up to 100% methanol and stored at -
193 20°C. Fins were rehydrated and then washed 3 x in PBS-Tx (0.02% Triton-X in PBS) for 10
194 mins before 6ermeabilization in PBS-Tx + proteinase K (1:1000, Sigma Aldrich (P5568)) at
195 37°C for 90 mins. Solutions were refreshed every 30 minutes. Samples were washed 3 x in
196 PBS-Tx for 10 mins and then blocked for 3 hours in blocking buffer (5% horse serum in
197 PBS) and incubated in primary antibody overnight at 4°C. Samples were washed in PBS-Tx
198 and blocked for 2 hours in blocking buffer staining with secondary antibody for 2 hours.
199 Primary antibodies: pAb to WNT16 (abcam, ab189033, 1:300), mAb to GFP (abcam,
200 ab13970, 1:500). The target human epitope of the polyclonal WNT16 primary antibody used
201 was 50-60% conserved in zebrafish Wnt16, with predicted cross-reactivity at the C-terminus
202 of the protein. Secondary antibodies: Alexa Fluor-647 and Alexa Fluor-488 (Thermo Fisher).
203 Steps were performed at room temperature unless stated otherwise. Samples were mounted
204 laterally in 1% agarose and imaged with a 10x objective lens on a SP5 confocal microscope
205 (Leica Microsystems).
206
207 *Whole-mount larval immunohistochemistry*
208
209 Larvae were euthanised in MS222 and fixed in 4% paraformaldehyde overnight at 4°C.
210 Larvae were dehydrated in a series of increasing concentrations up to 100% methanol and
211 stored at -20°C long-term until required. For staining, larvae were rehydrated and then
212 washed 3 x in PBS-Tw (0.1% TWEEN-20 in PBS) for 10 mins. Larvae were permeabilised in

bioRxiv preprint doi: https://doi.org/10.1101/2020.05.20.106328; this version posted May 21, 2020. The copyright holder for this preprint (which was not certified by peer review) is the author/funder, who has granted bioRxiv a license to display the preprint in perpetuity. It is made available under aCC-BY 4.0 International license.

213 PBS-Tw + proteinase K (1:1000) at 37°C for 25 mins (3 dpf) or 50 mins (5 dpf), with
214 solutions refreshed after 30 mins. Samples were washed 3 x in PBS-Tw for 10 mins each
215 and then blocked for 3 hours is blocking buffer before being stained and imaged as above.
216 Larvae were mounted ventrally, and the jaw region imaged. Primary antibodies: chick α–L-
217 plastin (gift from Martin lab [40]) and col2a1 (1:500, DSHB, M3F7). Secondary antibodies:
218 Alexa-488, DyLight 550 (Thermo Fisher).
219
220 *Tartrate-resistant acid phosphatase (TRAP) staining*
221
222 We used an Acid Phosphatase kit to detect osteoclast activity (Sigma-Aldrich, 387A).
223 Fractures were induced in WT and *wnt16*$^{-/-}$ *mpeg1*:mCherry zebrafish before being imaged
224 and amputated at 0 hpi, 24 hpi, 4 dpi and 7 dpi. Amputated fins were stored on ice then fixed
225 for 40 minutes at room temperature in TRAP-fix solution, comprised of 24% citrate solution
226 (from kit), 65% acetone, 8% formaldehyde (37%) and 3% deionized water. Samples were
227 washed in PBS-Tx 3 times. TRAP staining solution was prepared according to the kit
228 instructions. Each fin was placed in a separate well of a 24-well plate and incubated at 37°C
229 for 2 hours in 300 μl of TRAP stain. Fins were washed 3 times in PSB-Tx and post-fixed for
230 40 minutes at room temperature in 4% PFA before being transferred into 75% glycerol. Fins
231 were stored at 4°C before imaging on a stereomicroscope.
232
233 *Micro computed tomography (μCT)*
234
235 Adult fish were fixed in 4% PFA for 1 week followed by sequential dehydration to 70%
236 ethanol. Fish were scanned using a Bruker SKYSCAN 1227micro-CT scanner with a voxel
237 size of 5 μm, using an x-ray source of 60 keV, 50 W current and a 0.25mm thick aluminium
238 filter. Each scan acquired 1500 angular projections with 400 ms exposure time over a 180°
239 scan. X-radiographs were reconstructed using the filtered backprojection algorithm provided
240 by NRecon software (v. 1.7.1.0) and saved as 8-bit tiff stacks. "Phantom" samples of known
241 hydroxyapatite concentrations (0.25 and 0.75 g.cm^{-3} CaHA) were also scanned using
242 identical settings to calibrate estimates of bone mineral density (BMD) in the micro-CT fin
243 data.
244
245 *Tissue mineral density (TMD) analysis*
246
247 Avizo image analysis software (version 8.0, Thermo Fisher Scientific) was used to generate
248 3D volume renders of whole fins using a combination of automatic and manual

bioRxiv preprint doi: https://doi.org/10.1101/2020.05.20.106328; this version posted May 21, 2020. The copyright holder for this preprint (which was not certified by peer review) is the author/funder, who has granted bioRxiv a license to display the preprint in perpetuity. It is made available under aCC-BY 4.0 International license.

249 segmentation, which were saved as binary image stacks. The first 2 dorsal and ventral
250 lepidotrichia were excluded from the analysis of all fins due to varying resolution. Image
251 stacks were used to isolate the Greyscale values of segmented fins from values of
252 surrounding soft tissue and air by multiplying these binary (fin = 1; non-fin = 0) stacks
253 against the original reconstruction stacks using image algebra in Fiji/ImageJ [41]. Greyscale
254 values within resulting stacks, where values > 0 consisted solely of those representing fins,
255 were compared with the mean Greyscale values of both phantoms in order to calibrate the
256 TMD values that they represent.

257

258 *Fluorescent image analysis*

259

260 To quantify relative fluorescence intensities in fractures within transgenic fish, FIJI was used.
261 The average intensity for each fracture within a region of interest (ROI) was measured and
262 divided by the average intensity of uninjured bone in the same fish to give an “intensity
263 ratio”; this analysis method normalises for variability of reporter expression between fish and
264 allows for standardised comparison between individuals.

265

$$Intensity\ ratio = \frac{Average\ intensity\ of\ x\ within\ ROI\ at\ fracture\ site}{Average\ intensity\ of\ x\ in\ uninjured\ bone\ in\ the\ same\ fish}$$

266

$$x = stain\ or\ transgene\ reporter\ of\ interest\quad E.g.eGFP$$

267

268 To analyse the number of immune cells responding to fracture, we used the freely available
269 Modular Image Analysis (MIA; version 0.9.30) workflow automation plugin for Fiji [42-44].
270 Immune cell images were enhanced using the WEKA pixel classification plugin [45] and
271 thresholded at a probability of 0.5. Adjacent cells in the binarised image were separated
272 using an intensity-based watershed transform and individual cells subsequently identified as
273 regions of connected foreground-labelled pixels [46]. Cells were subjected to a size filter,
274 retaining only those in the range 30-500 μm^2. The distance of each cell to the manually
275 identified fracture site was measured.

276

277 *Statistical analysis*

278

279 Statistical analyses were performed, and graphs were created in GraphPad PRISM 8
280 software. Where possible, a D’Agostino Pearson normality test was performed on data to
281 determine whether a parametric or non-parametric statistical test should be used. Where two
282 or more data sets were compared, a One-way analysis of variance (ANOVA) or a Kruskal-

bioRxiv preprint doi: https://doi.org/10.1101/2020.05.20.106328; this version posted May 21, 2020. The copyright holder for this preprint (which was not certified by peer review) is the author/funder, who has granted bioRxiv a license to display the preprint in perpetuity. It is made available under aCC-BY 4.0 International license.

283 Wallis test was used to determine statistically significant differences between groups for
284 parametric and non-parametric data, respectively. For comparison of WT and *wnt16* mutants
285 throughout fracture repair, multiple t-tests were performed for each of the time points using
286 the Holm-Sidak correction to calculate P values. Differences were considered statistically
287 significant where $P < 0.05$.
288
289 **Results**
290
291 ***Young wnt16 mutant zebrafish are susceptible to spontaneous fractures which heal***
292 ***more slowly compared to wild type fish***
293
294 *WNT16* has been associated with low eBMD and increased fracture risk [15, 17, 47], whilst
295 *wnt16* mosaic mutant zebrafish displayed a low bone-mass phenotype [48]. Therefore, we
296 used μCT to observe bone morphology and tissue mineral density (TMD) in whole-fins of
297 adult WT and *wnt16*$^{-/-}$ zebrafish. *Wnt16* mutants displayed a high degree of variability in
298 TMD relative to WT specimens, as well as lower TMD (Figure 1 A-B). Images of *wnt16*$^{-/-}$ fins
299 showed a high frequency of bone calluses (Figure 1A), which form post-fracture and do not
300 completely resolve after the bone has repaired [29]. Bone calluses in the caudal fin rays can
301 be easily visualised using alizarin Red S (ARS). Thus, we next used ARS to compare the
302 frequency of spontaneous lepidotrichia fractures in young, 6 month old (mo) WT and 6 mo
303 *wnt16*$^{-/-}$ uninjured fish. Bone calluses and spontaneous fractures were rarely observed in the
304 6 mo WT fish, with only 25% of fish sampled displaying a minimal number of calluses (≤ 3)
305 (Figure 1 C-E). However, a significantly higher number of calluses were recorded in 6 mo
306 *wnt16*$^{-/-}$ fins; 100% of *wnt16*$^{-/-}$ fins sampled contained calluses, with a mean of 8.5 calluses
307 per fin versus 0.4 calluses per fin in WT. To test whether callus quantity increases with age,
308 we quantified callus number in 20 mo and 30 mo WT fish. Aged WT fish were comparable in
309 appearance and callus frequency to 6 mo *wnt16*$^{-/-}$ fish (Figure 1 C-E). Collectively, this
310 demonstrates that *wnt16*$^{-/-}$ fish display a bone fragility phenotype predisposing them to
311 spontaneous fractures and the accumulation of calluses at a young age.
312
313 ***New bone matrix is incorporated more slowly post-fracture in wnt16 mutant zebrafish***
314
315 Bone calluses are formed post-fracture; since *wnt16* mutants displayed variable TMD and a
316 high number of calluses, we next tested whether fracture repair was impaired in *wnt16*$^{-/-}$
317 zebrafish. Adult WT and *wnt16*$^{-/-}$ fish were live stained in ARS to label bone and imaged prior
318 to the induction of a fracture on a bone segment within the caudal lepidotrichia. Zebrafish
319 were then live stained in calcein green to label newly incorporated bone matrix at the

bioRxiv preprint doi: https://doi.org/10.1101/2020.05.20.106328; this version posted May 21, 2020. The copyright holder for this preprint (which was not certified by peer review) is the author/funder, who has granted bioRxiv a license to display the preprint in perpetuity. It is made available under aCC-BY 4.0 International license.

320 fracture site which was re-imaged at the time points indicated (Figure 1F). Injured *wnt16*$^{-/-}$
321 zebrafish displayed significantly reduced callus formation within the first 7 days of fracture
322 healing compared to WT, which was most apparent at 4 days post-injury (dpi) (Figure 1G
323 and H). We also investigated whether chondrocytes were involved in lepidotrichia bone
324 repair and if so, whether chondrocyte activity varied between WT and *wnt16* mutants.
325 Fractures were induced in the caudal fins of transgenic *col2a1*:mCherry zebrafish (Table 1)
326 and chondrocyte activity measured via fluorescence intensity. mCherry expression was
327 almost undetectable throughout fracture repair and intensity ratios showed little variation
328 from uninjured control bone at all time-points post-injury (Supplementary Figure S2 A-B).
329 Moreover, no significant differences in Col2a1 levels were observed between WT and *wnt16*
330 mutant fractures at any time point. This suggests that lepidotrichia fracture repair occurs
331 predominantly via an intramembranous route and that chondrocytes are not required for
332 adult bone repair in zebrafish.
333
334 ***Osteoblast recruitment is delayed in wnt16*$^{-/-}$ *zebrafish post-fracture***
335
336 Osteoblast activation is a key event in the bone repair process post-fracture. Osteoblasts
337 differentiate from mesenchymal stem cell (MSC) precursors expressing the transcription
338 factor osterix (*osx*) and synthesise bone matrix within the initial soft callus; the callus
339 hardens as it mineralises and is remodelled to restore the bone to a healthy state [49].
340 Moreover, transcriptomic analysis of osteoblast-prone clones isolated from tonsil derived
341 MSCs showed that upregulation of WNT16 is predictive of osteogenic differentiation [50]. In
342 zebrafish, osteoblasts dedifferentiate and proliferate in response to bone injury, migrating to
343 the damaged tissue where they initiate bone repair [28]. Thus, we next investigated whether
344 osteoblast number and distribution were impaired post-fracture repair in *wnt16*$^{-/-}$ zebrafish.
345 We performed live ARS prior to fin fractures of WT and *wnt16*$^{-/-}$ zebrafish carrying the
346 osteoblast-labelling transgene, *osx*:GFP (Table 1). Fractures were induced and re-stained
347 with live ARS at the time points indicated to ensure labelling of any new bone prior to
348 imaging (Figure 2A). The intensity of *osx*:GFP signal was measured as a ratio between the
349 fracture site and uninjured bone and used as a proxy for relative increases in osteoblast
350 number throughout fracture repair. In WT zebrafish, the number of osteoblasts at the
351 fracture site peaked rapidly at 4 dpi, before steadily decreasing (Figure 2B & C). However,
352 osteoblast number was significantly reduced at 4 dpi in *wnt16* mutants, not peaking until 10
353 dpi (Figure 2B & C). A comparable bony callus had formed at the fracture-site in both WT
354 and *wnt16*$^{-/-}$ by 15 dpi (Figure 2D). The delayed recruitment and reduced number of
355 osteoblasts at 4 dpi coincided with slower callus formation in *wnt16*$^{-/-}$ fractures (Figure 1 G-

bioRxiv preprint doi: https://doi.org/10.1101/2020.05.20.106328; this version posted May 21, 2020. The copyright holder for this preprint (which was not certified by peer review) is the author/funder, who has granted bioRxiv a license to display the preprint in perpetuity. It is made available under aCC-BY 4.0 International license.

356 H). This demonstrates that osteoblasts in *wnt16$^{-/-}$* zebrafish can respond to bone injury but
357 that the recruitment and activity of these osteoblasts are significantly delayed.
358

359 ***Activation of the canonical Wnt signalling pathway is enhanced at the fracture site in***
360 ***wnt16$^{-/-}$ zebrafish post-injury***
361

362 Wnt signalling proteins regulate the stemness, differentiation and proliferation of MSCs and
363 osteoblasts. Moreover, previous studies in mice have indicated that WNT16 may buffer
364 levels of canonical Wnt signalling in response to injury [12]. Therefore, we investigated
365 levels of canonical Wnt activity in *wnt16$^{-/-}$* zebrafish post-fracture using a β-catenin-
366 responsive transgenic line (Wnt:GFP (Table 1)). Fractures were induced in the caudal
367 lepidotrichia of the fish and imaged at identical time points as in Figure 2 A. In *wnt16$^{-/-}$*
368 zebrafish, we observed a significant increase in the area of canonical Wnt-responsive cells
369 at the fracture site from 2 dpi compared to WT (Figure 3). Canonical Wnt signalling remained
370 elevated in *wnt16$^{-/-}$* fractures through to 4 dpi, where Wnt:GFP intensity ratios were
371 comparable to WT fractures, before gradually decreasing to homeostatic levels by 10 dpi
372 (Figure 3B). Fractured fins from WT and *wnt16$^{-/-}$* Wnt:GFP^{+} zebrafish were amputated and
373 fixed 2 dpi and 4 dpi for immunohistochemistry to detect Wnt16, when the canonical Wnt
374 pathway was most active. Immunohistochemistry revealed high levels of Wnt16 at the
375 fracture site in WT zebrafish 2 dpi, coinciding with low levels of canonical Wnt pathway
376 activation (Supplementary Figure S3 A). This was proceeded by a loss of Wnt16 signal at
377 4dpi, where canonical Wnt activation increased. Conversely, *wnt16$^{-/-}$* mutants displayed high
378 levels of Wnt:GFP at both 4 and 7 dpi; only background levels of anti-Wnt16
379 immunolabelling were observed, which may be accounted for by antibody cross reactivity
380 with other proteins (Supplementary Figure S3 B). Collectively, this suggests that enhanced
381 canonical Wnt signalling underpins delayed callus formation and osteoblast differentiation in
382 response to fracture in *wnt16$^{-/-}$* zebrafish.
383

384 ***Innate immune cell dynamics are unaltered in wnt16$^{-/-}$ zebrafish post-fracture***
385

386 Fracture repair has been shown to comprise an inflammatory phase, a repair phase and a
387 remodelling phase in mammals [51]. The controlled recruitment, activity and reverse
388 migration of leukocytes during the inflammatory phase are known to be prerequisites for
389 initiating osteoblast activity and optimal bone repair [51, 52]. Neutrophils are known to be
390 amongst the first cells to be recruited to fractures to combat microbial infections and initiate
391 bone repair [24]; stimulation of non-canonical Wnt pathways with recombinant WNT5a has
392 been shown to initiate chemotactic migration and chemokine production in neutrophils, but

bioRxiv preprint doi: https://doi.org/10.1101/2020.05.20.106328; this version posted May 21, 2020. The copyright holder for this preprint (which was not certified by peer review) is the author/funder, who has granted bioRxiv a license to display the preprint in perpetuity. It is made available under aCC-BY 4.0 International license.

393 whether WNT16 influences neutrophil recruitment is unknown [53]. Macrophages also
394 rapidly respond to bone damage and continue to aid throughout the repair and remodelling
395 phases in mammalian models of fracture [23]. A previous study indicated that *wnt16*
396 expression was required for functional haematopoiesis in zebrafish embryos [21].
397 Additionally, overexpression of *WNT16* in mouse osteoblast-progenitor cells has been
398 shown to partially rescue glucocorticoid-induced osteoporosis [54], suggesting that Wnt16
399 may regulate osteoblast activity and bone repair via immune cells. To validate whether early
400 leukocyte development was impaired in *wnt16* mutants, we fixed zebrafish larvae at 3 and 5
401 days post-fertilization (dpf). Whole-mount immunohistochemistry was used to label cartilage
402 in the developing skeleton (Col2a1) and immune cells (L-plastin) but surprisingly, no
403 differences in leukocyte numbers were observed at either age (Supplementary Figure S4).
404 Despite this, since callus formation and osteoblast differentiation were delayed in *wnt16*$^{-/-}$
405 fractures, we also investigated whether immune cell recruitment to bone injury was altered in
406 adult *wnt16* mutants. To this end, we used the *lyzC*:DsRed (neutrophils) and
407 *mpeg1*:mCherry (macrophages) transgenic zebrafish lines (Table 1) to study leukocyte
408 dynamics post-fracture in WT and *wnt16*$^{-/-}$ zebrafish. Immune cell recruitment relative to the
409 fracture site over time was quantified using modular image analysis [42]. The number of
410 neutrophils (*lyzC*$^{+}$ cells) and macrophages (*mpeg1*$^{+}$ cells) within a 100 μm radius and 300
411 μm radius of the fracture were calculated (Figure 4 A). In both WT and *wnt16*$^{-/-}$ fish,
412 neutrophils were rapidly recruited to the fracture, peaking between 8 and 24 hpi (Figure 4 B).
413 No significant differences in the number of neutrophils recruited to the fracture sites of WT
414 and *wnt16*$^{-/-}$ zebrafish were detected at any time point post-injury (Figure 4 C-D).
415 Macrophages were also rapidly recruited to fractures in the first 24 hpi (Figure 4 E).
416 Interestingly, we observed that macrophages responded to fracture in a biphasic manner,
417 decreasing in number from 2-4 dpi, before peaking in number for a second time around 7 dpi
418 (Figure 4 F-G). This suggests that phenotypically distinct populations of macrophages may
419 be required at different stages post-fracture to contribute to efficient bone repair.
420 Comparison between WT and *wnt16*$^{-/-}$ zebrafish showed no difference in the number of
421 *mpeg1*$^{+}$ cells recruited to the fracture throughout repair, aside from a significant increase in
422 macrophage number in *wnt16*$^{-/-}$ zebrafish at 8hpi (Figure 4 F-G). These data suggest that,
423 overall, leukocyte recruitment to fractures is not impaired in *wnt16* mutants and does not
424 contribute to delayed bone repair resulting from loss of Wnt16.
425
426 ***Patterning of TRAP activity is altered in wnt16*$^{-/-}$ *zebrafish***
427

bioRxiv preprint doi: https://doi.org/10.1101/2020.05.20.106328; this version posted May 21, 2020. The copyright holder for this preprint (which was not certified by peer review) is the author/funder, who has granted bioRxiv a license to display the preprint in perpetuity. It is made available under aCC-BY 4.0 International license.

428 TRAP-synthesising osteoclasts are required to resorb damaged bone but must be regulated
429 to prevent osteoporosis. Recombinant WNT16 has been shown to supress
430 osteoclastogenesis and TRAP activity *in vitro* by regulating osteoprotegerin expression in
431 osteoblasts [55]. The uptake of osteoblast-derived extracellular vesicles by immature
432 osteoclasts has been shown to promote osteoclast differentiation in zebrafish scale
433 fractures, demonstrating that intercellular communication between osteoblasts and
434 osteoclasts regulates osteoclastogenesis in response to bone damage [56]. Osteoclasts and
435 macrophages are derived from a common myeloid lineage, with peripheral blood monocytes
436 showing higher osteoclastic potential compared to bone marrow derived monocytes [57].
437 Moreover, a previous study established that cells expressing the osteoclast marker
438 cathepsin K infiltrate the lepidotrichia fracture site where TRAP is detected by 24 hpi in
439 zebrafish [29]; this coincides with the recruitment of the initial wave of *mpeg1*-expressing
440 cells to the fracture site observed in our model (Figure 4 E-G). Therefore, we investigated
441 whether TRAP activity post-fracture was associated with the recruitment of *mpeg*$^+$ cells and
442 whether loss of Wnt16 affected levels of TRAP. Fractures were induced in *mpeg1*:mCherry$^+$
443 WT and *wnt16*$^{-/-}$ zebrafish and live-imaged prior to amputation of the fin for TRAP staining.
444 The overall levels of osteoclast activity were measured by calculating percentage area of
445 TRAP$^+$-stained tissue within 300 µm radius of the fracture site. Osteoclast activity increased
446 rapidly at 24 hpi and remained high before gradually decreasing by 7 dpi (Figure 5 A-B). No
447 significant difference in overall levels of osteoclast activity at the fracture site (TRAP$^+$ %
448 area) was detected between WT and *wnt16*$^{-/-}$ fractures (Figure 5 B). However, the overall
449 patterning of TRAP staining was altered at 24 hpi and 7 dpi; *wnt16*$^{-/-}$ zebrafish displayed a
450 significantly higher number of TRAP$^+$ punctae around the fracture, whereas WT fractures
451 tended to display fewer punctae, with continuous, diffuse areas of TRAP$^+$ tissue (Figure 5 A
452 & C). Comparable patterning of TRAP$^+$ punctae was not observed in uninjured bone from
453 either WT *wnt16* mutants. Interestingly, we observed similarities in the patterning of TRAP$^+$
454 punctae and *mpeg1*$^+$ cells, with punctae colocalising with *mpeg1*$^+$ expression in some
455 regions (Supplementary figure 5). This suggests that *mpeg1*-expressing cells may contribute
456 to bone remodelling and TRAP-synthesis during the early stages of fracture repair.
457
458 **Discussion**
459
460 Multiple studies have associated mutations in *WNT16* with osteoporosis and fracture
461 susceptibility phenotypes in humans [15-17], but less was known about the
462 pathophysiological influence of *WNT16* on bone and fracture repair. Moreover, models to
463 study the influence of GWAS-derived fracture-susceptibility candidate genes on bone
464 dynamically *in vivo* were lacking. In this study, we show that loss of Wnt16 in zebrafish leads

bioRxiv preprint doi: https://doi.org/10.1101/2020.05.20.106328; this version posted May 21, 2020. The copyright holder for this preprint (which was not certified by peer review) is the author/funder, who has granted bioRxiv a license to display the preprint in perpetuity. It is made available under aCC-BY 4.0 International license.

465 to variable TMD and the accumulation of bone calluses within lepidotrichia resulting from
466 fractures at an early age. Induction of fractures in caudal fin lepidotrichia and subsequent
467 live imaging showed that Wnt16 is required for optimal fracture healing and the rapid
468 proliferation of osteoblasts post-injury. This coincided with prolonged activation of the
469 canonical Wnt signalling pathway in *wnt16* mutants. Overall, we found that loss of Wnt16 did
470 not impair the development of leukocytes or the responsiveness of neutrophils and
471 macrophages to bone injury but does alter the patterning of TRAP activity at the fracture
472 site.
473
474 Disordered activation of the canonical Wnt signalling pathway has been linked to the
475 pathogeneses of many age-related diseases such as cancer, cardiovascular disease,
476 osteoarthritis and osteoporosis [58]. It is thought that WNT16 may antagonise canonical Wnt
477 activity; WNT16 was found to be protective against excessive activation of canonical WNT
478 and severe cartilage degeneration in an induced osteoarthritis murine model [12]. Canonical
479 Wnt signalling culminates in the accumulation of β-catenin in the cell which translocates to
480 the nucleus where it binds to and activates the transcription factors, TCF/LEF (T cell
481 factor/lymphoid-enhancing binding factor). Whilst canonical Wnt signalling is required for
482 osteogenesis, LEF-1 is downregulated in the early stages of fracture repair during soft callus
483 formation [59]. It has been shown that constitutive β-catenin mediated activation of LEF-1
484 represses the osteoblast transcriptional regulator, Runx-2 and subsequent of expression
485 osteocalcin in osteoblasts [60]. This suggests that delayed callus formation post-fracture in
486 *wnt16*$^{-/-}$ zebrafish is due to overactivation of the canonical Wnt signalling pathway which
487 supresses osteoblast differentiation and bone matrix production.
488
489 In contrast to *wnt16* morphant embryos in Clements *et al.*, which displayed severe
490 impairment of haematopoiesis [21], we found that loss of Wnt16 had no effect on the overall
491 number of leukocytes detected in larvae during early skeletogenesis, nor did it have an
492 overall effect on the recruitment of neutrophils and macrophages post-fracture. Evidence
493 has shown that gene knockdown using morpholinos can have off-target effects which are
494 hard to control for and show more extreme phenotypes compared to stable mutant lines [61].
495 Our data demonstrates that targeted, stable loss of Wnt16 via CRISPR-Cas9 mutagenesis
496 does not impair early leukocyte haematopoiesis or the innate immune response to bone
497 injury in adult tissues.
498
499 Our data suggests that fracture repair in zebrafish lepidotrichia comprises 3 phases, similarly
500 to mammals [51]. The first is an initial inflammatory phase (~4-48 hpi) whereby neutrophils

bioRxiv preprint doi: https://doi.org/10.1101/2020.05.20.106328; this version posted May 21, 2020. The copyright holder for this preprint (which was not certified by peer review) is the author/funder, who has granted bioRxiv a license to display the preprint in perpetuity. It is made available under aCC-BY 4.0 International license.

501 and macrophages infiltrate the fracture. This is proceeded by a repair phase (~3-10 dpi)
502 whereby osteoblasts are activated and synthesise new bone matrix to unionise the fracture
503 with a callus. Ultimately, the bone enters an ongoing remodelling phase (>10 dpi) in which,
504 like humans, the repaired bone remains marked with a calcified callus. Moreover, the
505 biphasic response of macrophage recruitment we observed for the first time in zebrafish is
506 reminiscent of mammalian bone repair, whereby M1-like macrophages are observed during
507 the inflammatory phase and replaced by reparative M2-like macrophages which contribute
508 towards bone matrix synthesis and remodelling of bone [23, 57, 62]. Interestingly, we
509 observed the presence of TRAP$^+$ punctae at the fracture site, which coincided with the
510 recruitment of *mpeg1*$^+$ macrophages. This suggests that *mpeg1*$^+$ cells recruited to the
511 fractures may differentiate into osteoclasts. Indeed, monocytes are known to differentiate
512 into osteoclasts under pro-inflammatory conditions in mammals, whilst Wnt16 has been
513 shown to inhibit the differentiation of bone marrow cells into osteoclasts *in vitro* [22, 55].
514 Recently, evidence has emerged demonstrating that *mpeg1* expression is not restricted to
515 macrophages in adult zebrafish, as a large proportion of *mpeg1*$^+$ cells were found to be B
516 cells [63]. The number of TRAP$^+$ punctae at the fracture site 24 hpi and 4 dpi was
517 significantly higher in *wnt16* mutants compared to WT. Taken together, this data poses the
518 possibility that *mpeg1* is expressed by other HSC-derived lineages such as osteoclasts, the
519 differentiation of which may be regulated by Wnt16. However, whether distinct sub-
520 populations of macrophages contribute differentially throughout fracture repair in zebrafish
521 requires further investigation.
522
523 Though the presence of glycosaminoglycans has been previously reported in the early
524 stages post-injury in a zebrafish fracture model [29], we observed no marked increase in
525 chondrocyte activity throughout fracture repair in the caudal fins of *col2a1*:mCherry
526 zebrafish. This suggests that lepidotrichia bone repair in zebrafish occurs predominantly via
527 intramembranous ossification as opposed to endochondral ossification, unlike mammalian
528 bones, which utilise both mechanisms [64]. Despite this, our study helps to establish
529 zebrafish as a strong, emerging model for studying factors influencing the dynamic
530 behaviour of the multiple cell-types underpinning fracture repair and bone pathologies *in*
531 *vivo*. By studying the lepidotrichia in the transparent fins of live zebrafish, we were able to
532 visualise bone fragility phenotypes in a novel *wnt16*$^{-/-}$ mutant as well as the influence of
533 *wnt16* on bone repair in a dynamic, longitudinal manner. Using this model, we found
534 evidence to suggest that the osteoporosis-associated gene *wnt16* elicits a protective effect
535 against fracture susceptibility and promotes bone repair by buffering levels of canonical Wnt
536 activity to promote optimal osteoblast activity.
537

bioRxiv preprint doi: https://doi.org/10.1101/2020.05.20.106328; this version posted May 21, 2020. The copyright holder for this preprint (which was not certified by peer review) is the author/funder, who has granted bioRxiv a license to display the preprint in perpetuity. It is made available under aCC-BY 4.0 International license.

538 **Supplementary materials**

539

540 Supplementary figures S1-5.

541

542 **Materials availability**

543

544 Mutant *wnt16*$^{-/-}$ zebrafish available upon request to the lead contact.

545

546

547 **Data availability**

548

549 Imaging data will be made available through the university of Bristol's RDSF server.

550

551 **Lead contact**

552

553 Further information and requests for materials associated with this study should be directed
554 to and will be made available upon reasonable request by the lead contact, Chrissy
555 Hammond: chrissy.hammond@bristol.ac.uk.

556

557 **Funding**

558

559 LMM was funded by Wellcome Trust Dynamic Molecular Cell Biology PhD Programme at
560 the University of Bristol (108907/Z/15/Z); EK and CLH were funded by Versus Arthritis
561 Senior Research Fellowship (29137).

562

563 **Author contributions**

564

565 Experimental design: LMM, EK, CLH. Conducting experiments: LMM, EK, AV. Image
566 analysis: LMM, AV, SC, EN. Statistical analysis: LMM. Manuscript: LMM, EK, CLH.

567

568 **Acknowledgements**

569

570 We would like to thank Mathew Green and technical staff at the zebrafish aquarium within
571 the University of Bristol's Animal Scientific Unit for providing animal husbandry and
572 management. We gratefully acknowledge the Wolfson Bioimaging Facility for imaging
573 support.

574

bioRxiv preprint doi: https://doi.org/10.1101/2020.05.20.106328; this version posted May 21, 2020. The copyright holder for this preprint (which was not certified by peer review) is the author/funder, who has granted bioRxiv a license to display the preprint in perpetuity. It is made available under aCC-BY 4.0 International license.

575 **Conflict of Interest Statement**

576

577 The authors declare no conflict of interest.

578

579 **Figure Legends**

580

581 **Figure 1. *wnt16* mutants are susceptible to lepidotrichia bone fractures which heal
582 more slowly compared to wild type zebrafish. A:** micro-CT images indicate lower and
583 more variable tissue mineral density (TMD) and the presence of bone calluses (arrowheads)
584 in the fins of *wnt16*$^{-/-}$ zebrafish. **B:** Violin plots show distribution around mean (black line)
585 TMD in wild type (WT) and *wnt16*$^{-/-}$ fins. n= 3, scale bar = 1 mm. **C:** Uninjured WT and
586 *wnt16*$^{-/-}$ zebrafish were live-stained with alizarin red at 6, 20 or 30 months old (mo). Scale =
587 1 mm. **D:** Higher magnification of fins (from C) shows the presence of bone calluses
588 (arrowheads) resulting from bone repair in 6 mo *wnt16*$^{-/-}$ and 30 mo WT zebrafish but not 6
589 mo zebrafish. Scale = 200 µm. **E:** Quantification of bone calluses per fin shows that young
590 *wnt16* mutants display a significantly higher number of calluses compared to WT fish at the
591 same age but no significant difference compared with aged WT zebrafish. n ≥ 5 per
592 condition. **F:** Schematic illustrating fracture induction assay and labelling of old bone
593 (Alizarin R) and new bone (calcein green). **G:** Callus formation was quantified by measuring
594 the calcein intensity ratio between the fracture-site and uninjured bone. Callus formation was
595 significantly reduced from 2-7 days post-injury (dpi) in *wnt16* mutant compared to WT
596 fractures. n ≥ 5 per condition. Grey dotted line indicates where calcein intensity at the
597 fracture site = uninjured bone **H:** Representative images of WT and *wnt16*$^{-/-}$ fish at selected
598 time points post-injury show old bone labelled by Alizarin R (grey) and callus formation
599 labelled by calcein (magenta = low intensity, yellow = high intensity). White asterisk = centre
600 of fracture. Scale 200 µm. n.s = no significant difference, * = P < 0.05, ** = P < 0.01, **** = P
601 < 0.0001.

602

603 **Figure 2. Osteoblast recruitment is significantly delayed post-fracture in *wnt16*$^{-/-}$
604 zebrafish. A:** Schematic illustrating induced-fracture time course and days post-injury (dpi)
605 in which *osx*:GFP zebrafish immersed in Alizarin Red (magenta) for bone labelling and
606 imaged. **B:** Representative images of calcified bone (Alizarin red) and osteoblasts (*osx*:GFP)
607 at fracture site in wild type (WT) and *wnt16*$^{-/-}$ throughout fracture repair. White asterisk =
608 centre of fracture. Scale bar = 200 µm. **C:** Osteoblast number was quantified by measuring
609 the fluorescence intensity of *osx*:GFP within the fracture site normalised to control bone in
610 the same fin (intensity ratio). Grey dotted line indicates where osteoblast number at the

bioRxiv preprint doi: https://doi.org/10.1101/2020.05.20.106328; this version posted May 21, 2020. The copyright holder for this preprint (which was not certified by peer review) is the author/funder, who has granted bioRxiv a license to display the preprint in perpetuity. It is made available under aCC-BY 4.0 International license.

611 fracture site = uninjured bone. Osteoblast recruitment was delayed in *wnt16*$^{-/-}$ mutants, which
612 had significantly fewer osteoblasts at the fracture site 4 dpi, but significantly more
613 osteoblasts at 10 dpi compared to WT zebrafish. * = $P < 0.05$, ** = $P < 0.01$. n = 6 per
614 genotype. **D:** Confocal imaging of bone in amputated fins at the end of the time course (15
615 dpi) shows complete union of fractures in both WT and *wnt16*$^{-/-}$ zebrafish. Scale bar = 100
616 µm.
617
618 **Figure 3. The Canonical Wnt pathway is over-activated in the early stages of fracture**
619 **repair in *wnt16*$^{-/-}$ zebrafish A:** Fractures were induced in *wnt*:GFP transgenic zebrafish
620 which express GFP in cells responding to activation of the canonical Wnt signalling pathway.
621 Representative images are shown from 0, 2, 4 and 7 days post-fracture (dpi). Dotted line =
622 bone outline, White asterisk = centre of fracture. Scale bar = 200 µm. **B:** Levels of Wnt
623 pathway activation throughout fracture repair were quantified by measuring the fluorescence
624 intensity of Wnt:GFP within the fracture site normalised to control bone in the same fin
625 (intensity ratio). Grey dotted line indicates where canonical Wnt activity at the fracture site =
626 uninjured bone. *wnt16*$^{-/-}$ zebrafish displayed significantly higher levels of canonical Wnt
627 activity at 2 dpi compared to WT fractures. High levels of Wnt:GFP at the fracture site were
628 sustained through to 4 dpi in *wnt16* mutants where they became comparable with WT. **** =
629 $P < 0.0001$. n ≥ 6 per genotype.
630
631 **Figure 4. Loss of Wnt16 does not perturb leukocyte recruitment to bone post-fracture.**
632 Fractures were induced in wild type (WT) and *wnt16*$^{-/-}$ zebrafish carrying *lyzC*:DsRed and
633 *mpeg1*:mCherry transgenes to measure the recruitment of neutrophils and macrophages,
634 respectively. **A:** Schematic depicting regions of interest around the fracture site where
635 leukocyte recruitment was quantified. **B:** Representative images of from WT and *wnt16*$^{-/-}$
636 zebrafish show neutrophil (*lyzC*$^{+}$ cells) recruitment to fractured bone at 0, 8 and 24 hours
637 post-injury (hpi) and 7 days post-injury (dpi). Scale bar = 100 µm. **C & D:** The number of
638 neutrophils within 100 µm (C) and 300 µm (D) of the fractures were quantified in an
639 automated manner using modular image analysis (MIA) from 0 hpi to 14 dpi. WT and wnt16
640 mutants displayed comparable numbers of neutrophils at the fracture site at all time-points
641 post-injury. n ≥ 5 per genotype **E:** Representative images of from WT and *wnt16*$^{-/-}$ zebrafish
642 show macrophage (mpeg1^{+} cells) recruitment to fractured bone at selected time points from
643 0-14 dpi. Scale bar = 100 µm. **F & G:** The number of neutrophils within 100 µm (F) and 300
644 µm (G) of the fractures were quantified using MIA from 0 hpi to 14 dpi. WT and wnt16
645 mutants displayed comparable numbers of macrophages at all time-points post-injury, with

bioRxiv preprint doi: https://doi.org/10.1101/2020.05.20.106328; this version posted May 21, 2020. The copyright holder for this preprint (which was not certified by peer review) is the author/funder, who has granted bioRxiv a license to display the preprint in perpetuity. It is made available under aCC-BY 4.0 International license.

646 the exception of 8 hpi when *wnt16* mutants had recruited significantly more macrophages to
647 within 100 μm of the fracture site (F). * = P < 0.05. n ≥ 5 per genotype.
648

649 **Figure 5. TRAP$^+$ punctae accumulate near to fractures in *wnt16$^{-/-}$* zebrafish post-injury.**
650 Fins from wild type (WT) and *wnt16$^{-/-}$* zebrafish were amputated at 0 hours post-fracture
651 (hpi), 24 hpi, 4 days post-fracture (dpi) and 7 dpi before undergoing staining to detect the
652 presence of tartrate-resistant acid phosphatase (TRAP). **A:** Representative images of
653 fractures stained for TRAP. Scale bar = 100 *μ*m **B:** Overall coverage of TRAP was
654 measured by calculating the total % area stained within 300 μm of the fracture site. No
655 significant difference in the amount of TRAP$^+$ stained area between WT and *wnt16$^{-/-}$*
656 fractures was found. **C:** The number of TRAP$^+$ punctae present within 300 μm of the fracture
657 site were quantified and showed a significantly higher number of punctae at 24 hpi and 4 dpi
658 in the fractures of *wnt16$^{-/-}$* zebrafish compared to WT. * = P < 0.05. n ≥ 6 per genotype.
659

660 **References**

661

662 1. Su, N., Yang, J., Xie, Y.L., Du, X.L., Chen, H.G., Zhou, H., and Chen, L. (2019). Bone
663 function, dysfunction and its role in diseases including critical illness. International
664 Journal of Biological Sciences *15*, 776-787.
665 2. Sinder, B.P., Pettit, A.R., and McCauley, L.K. (2015). Macrophages: Their Emerging
666 Roles in Bone. Journal of Bone and Mineral Research *30*, 2140-2149.
667 3. Drake, M.T., Clarke, B.L., and Lewiecki, E.M. (2015). The Pathophysiology and
668 Treatment of Osteoporosis. Clinical Therapeutics *37*, 1837-1850.
669 4. Raggatt, L.J., and Partridge, N.C. (2010). Cellular and Molecular Mechanisms of Bone
670 Remodeling. Journal of Biological Chemistry *285*, 25103-25108.
671 5. Chen, D., Shen, J., Zhao, W.W., Wang, T.Y., Han, L., Hamilton, J.L., and Im, H.J. (2017).
672 Osteoarthritis: toward a comprehensive understanding of pathological mechanism.
673 Bone Research *5*.
674 6. Johnell, O., Kanis, J.A., Oden, A., Johansson, H., De Laet, C., Delmas, P., Eisman, J.A.,
675 Fujiwara, S., Kroger, H., Mellstrom, D., et al. (2005). Predictive value of BMD for hip
676 and other fractures. Journal of Bone and Mineral Research *20*, 1185-1194.
677 7. National Osteoporosis Society. (2017). NHS RightCare scenario:The variation
678 between sub-optimal and optimal pathways.
679 8. Houschyar, K.S., Tapking, C., Borrelli, M.R., Popp, D., Duscher, D., Maan, Z.N.,
680 Chelliah, M.P., Li, J.T., Harati, K., Wallner, C., et al. (2019). Wnt Pathway in Bone
681 Repair and Regeneration - What Do We Know So Far. Frontiers in Cell and
682 Developmental Biology *6*.
683 9. Nusse, R. (2005). Wnt signaling in disease and in development. Cell Research *15*, 28-
684 32.
685 10. Komiya, Y., and Habas, R. (2008). Wnt signal transduction pathways. Volume 4.
686 (*Organogenesis*), pp. 68–75.

bioRxiv preprint doi: https://doi.org/10.1101/2020.05.20.106328; this version posted May 21, 2020. The copyright holder for this preprint (which was not certified by peer review) is the author/funder, who has granted bioRxiv a license to display the preprint in perpetuity. It is made available under aCC-BY 4.0 International license.

687 11. Kobayashi, Y., Uehara, S., and Udagawa, N. (2018). Roles of non-canonical Wnt
688 signaling pathways in bone resorption. Journal of Oral Biosciences *60*, 31-35.
689 12. Nalesso, G., Thomas, B.L., Sherwood, J.C., Yu, J., Addimanda, O., Eldridge, S.E.,
690 Thorup, A.S., Dale, L., Schett, G., Zwerina, J., et al. (2017). WNT16 antagonises
691 excessive canonical WNT activation and protects cartilage in osteoarthritis. Annals of
692 the Rheumatic Diseases *76*, 218-226.
693 13. Gori, F., Lerner, U., Ohlsson, C., and Baron, R. (2015). A new WNT on the bone:
694 WNT16, cortical bone thickness, porosity and fractures. Bonekey Reports *4*.
695 14. Tachmazidou, I., Hatzikotoulas, K., Southam, L., Esparza-Gordillo, J., Haberland, V.,
696 Zheng, J., Johnson, T., Koprulu, M., Zengini, E., Steinberg, J., et al. (2019).
697 Identification of new therapeutic targets for osteoarthritis through genome-wide
698 analyses of UK Biobank data. Nature Genetics *51*, 231-236.
699 15. Morris, J.A., Kemp, J.P., Youlten, S.E., Laurent, L., Logan, J.G., Chai, R.C., Vulpescu,
700 N.A., Forgetta, V., Kleinman, A., Mohanty, S.T., et al. (2019). An atlas of genetic
701 influences on osteoporosis in humans and mice. Nature Genetics.
702 16. Koller, D.L., Zheng, H.F., Karasik, D., Yerges-Armstrong, L., Liu, C.T., McGuigan, F.,
703 Kemp, J.P., Giroux, S., Lai, D.B., Edenberg, H.J., et al. (2013). Meta-analysis of
704 genome-wide studies identifies WNT16 and ESR1 SNPs associated with bone mineral
705 density in premenopausal women. Journal of Bone and Mineral Research *28*, 547-
706 558.
707 17. Zheng, H.F., Tobias, J.H., Duncan, E., Evans, D.M., Eriksson, J., Paternoster, L., Yerges-
708 Armstrong, L.M., Lehtimaki, T., Bergstrom, U., Kahonen, M., et al. (2012). WNT16
709 Influences Bone Mineral Density, Cortical Bone Thickness, Bone Strength, and
710 Osteoporotic Fracture Risk. Plos Genetics *8*.
711 18. Alam, I., Alkhouli, M., Gerard-O'Riley, R.L., Wright, W.B., Acton, D., Gray, A.K., Patel,
712 B., Reilly, A.M., Lim, K.E., Robling, A.G., et al. (2016). Osteoblast-Specific
713 Overexpression of Human WNT16 Increases Both Cortical and Trabecular Bone Mass
714 and Structure in Mice. Endocrinology *157*, 722-736.
715 19. Alam, I., Oakes, D., Sbeta, S., Billingsley, C., Acton, D., Reilly, A., Gerard-O'Riley, R.,
716 and Econs, M. (2017). Overexpression of WNT16 does not Rescue the Bone Loss due
717 to Glucocorticoid Treatment in Mice. Journal of Bone and Mineral Research *32*,
718 S370-S370.
719 20. Geurtzen, K., Vernet, A., Freidin, A., Rauner, M., Hofbauer, L.C., Schneider, J.E.,
720 Brand, M., and Knopf, F. (2017). Immune Suppressive and Bone Inhibitory Effects of
721 Prednisolone in Growing and Regenerating Zebrafish Tissues. Journal of Bone and
722 Mineral Research *32*, 2476-2488.
723 21. Clements, W.K., Kim, A.D., Ong, K.G., Moore, J.C., Lawson, N.D., and Traver, D.
724 (2011). A somitic Wnt16/Notch pathway specifies haematopoietic stem cells. Nature
725 *474*, 220-U262.
726 22. Lampiasi, N., Russo, R., and Zito, F. (2016). The Alternative Faces of Macrophage
727 Generate Osteoclasts. Biomed Research International.
728 23. Raggatt, L.J., Wullschleger, M.E., Alexander, K.A., Wu, A.C.K., Millard, S.M., Kaur, S.,
729 Maugham, M.L., Gregory, L.S., Steck, R., and Pettit, A.R. (2014). Fracture Healing via
730 Periosteal Callus Formation Requires Macrophages for Both Initiation and
731 Progression of Early Endochondral Ossification. American Journal of Pathology *184*,
732 3192-3204.

bioRxiv preprint doi: https://doi.org/10.1101/2020.05.20.106328; this version posted May 21, 2020. The copyright holder for this preprint (which was not certified by peer review) is the author/funder, who has granted bioRxiv a license to display the preprint in perpetuity. It is made available under aCC-BY 4.0 International license.

733 24. Bastian, O.W., Koenderman, L., Alblas, J., Leenen, L.P.H., and Blokhuis, T.J. (2016).
734 Neutrophils contribute to fracture healing by synthesizing fibronectin(+) extracellular
735 matrix rapidly after injury. Clinical Immunology *164*, 78-84.
736 25. Kettleborough, R.N.W., Busch-Nentwich, E.M., Harvey, S.A., Dooley, C.M., de Bruijn,
737 E., van Eeden, F., Sealy, I., White, R.J., Herd, C., Nijman, I.J., et al. (2013). A
738 systematic genome-wide analysis of zebrafish protein-coding gene function. Nature
739 *496*, 494-+.
740 26. Bergen, D.J.M., Kague, E., and Hammond, C.L. (2019). Zebrafish as an Emerging
741 Model for Osteoporosis: A Primary Testing Platform for Screening New Osteo-Active
742 Compounds. Frontiers in Endocrinology *10*.
743 27. Novoa, B., and Figueras, A. (2012). Zebrafish: Model for the Study of Inflammation
744 and the Innate Immune Response to Infectious Diseases. Current Topics in Innate
745 Immunity Ii *946*, 253-275.
746 28. Geurtzen, K., Knopf, F., Wehner, D., Huitema, L.F.A., Schulte-Merker, S., and
747 Weidinger, G. (2014). Mature osteoblasts dedifferentiate in response to traumatic
748 bone injury in the zebrafish fin and skull. Development *141*, 2225-2234.
749 29. Tomecka, M.J., Ethiraj, L.P., Sanchez, L.M., Roehl, H.H., and Carney, T.J. (2019).
750 Clinical pathologies of bone fracture modelled in zebrafish. Disease Models &
751 Mechanisms *12*.
752 30. Westerfield, M. (2000). The zebrafish book: a guide for the laboratory use of
753 zebrafish (Danio rerio) 4th Edition, (Eugene, OR, USA: University of Oregon Press).
754 31. Alestrom, P., D'Angelo, L., Midtlyng, P.J., Schorderet, D.F., Schulte-Merker, S., Sohm,
755 F., and Warner, S. Zebrafish: Housing and husbandry recommendations. Laboratory
756 Animals.
757 32. Moro, E., Ozhan-Kizil, G., Mongera, A., Beis, D., Wierzbicki, C., Young, R.M., Bournele,
758 D., Domenichini, A., Valdivia, L.E., Lum, L., et al. (2012). In vivo Wnt signaling tracing
759 through a transgenic biosensor fish reveals novel activity domains. Developmental
760 Biology *366*, 327-340.
761 33. DeLaurier, A., Eames, B.F., Blanco-Sanchez, B., Peng, G., He, X.J., Swartz, M.E.,
762 Ullmann, B., Westerfield, M., and Kimmel, C.B. (2010). Zebrafish sp7:EGFP: A
763 Transgenic for Studying Otic Vesicle Formation, Skeletogenesis, and Bone
764 Regeneration. Genesis *48*, 505-511.
765 34. Mitchell, R.E., Huitema, L.F.A., Skinner, R.E.H., Brunt, L.H., Severn, C., Schulte-
766 Merker, S., and Hammond, C.L. (2013). New tools for studying osteoarthritis genetics
767 in zebrafish. Osteoarthritis and Cartilage *21*, 269-278.
768 35. Ellett, F., Pase, L., Hayman, J.W., Andrianopoulos, A., and Lieschke, G.J. (2011).
769 mpeg1 promoter transgenes direct macrophage-lineage expression in zebrafish.
770 Blood *117*, E49-E56.
771 36. Hall, C., Flores, M.V., Storm, T., Crosier, K., and Crosier, P. (2007). The zebrafish
772 lysozyme C promoter drives myeloid-specific expression in transgenic fish. Bmc
773 Developmental Biology *7*.
774 37. Brunt, L.H., Begg, K., Kague, E., Cross, S., and Hammond, C.L. (2017). Wnt signalling
775 controls the response to mechanical loading during zebrafish joint development.
776 Development *144*, 2798-2809.
777 38. Bensimon-Brito, A., Cardeira, J., Dionisio, G., Huysseune, A., Cancela, M.L., and
778 Witten, P.E. (2016). Revisiting in vivo staining with alizarin red S - a valuable

bioRxiv preprint doi: https://doi.org/10.1101/2020.05.20.106328; this version posted May 21, 2020. The copyright holder for this preprint (which was not certified by peer review) is the author/funder, who has granted bioRxiv a license to display the preprint in perpetuity. It is made available under aCC-BY 4.0 International license.

779 approach to analyse zebrafish skeletal mineralization during development and
780 regeneration. Bmc Developmental Biology *16*.
781 39. Stuart, A.J., and Smith, D.A. (1992). Use Of The Fluorochromes Xylenol Orange,
782 Calcein Green, And Tetracycline To Document Bone Deposition And Remodeling In
783 Healing Fractures In Chickens. Avian Diseases *36*, 447-449.
784 40. Cvejic, A., Hall, C., Bak-Maier, M., Flores, M.V., Crosier, P., Redd, M.J., and Martin, P.
785 (2008). Analysis of WASp function during the wound inflammatory response - live-
786 imaging studies in zebrafish larvae. Journal of Cell Science *121*, 3196-3206.
787 41. Tommasini, S.M., Trinward, A., Acerbo, A.S., De Carlo, F., Miller, L.M., and Judex, S.
788 (2012). Changes in intracortical microporosities induced by pharmaceutical
789 treatment of osteoporosis as detected by high resolution micro-CT. Bone *50*, 596-
790 604.
791 42. Cross, S.J. (2019). SJCross/MIA: Version 0.9.30 (Version v0.9.30). Volume 2020,
792 06/12/2019 Edition. (https://github.com/SJCross/MIA: Zenodo).
793 43. Rueden, C.T., Schindelin, J., Hiner, M.C., DeZonia, B.E., Walter, A.E., Arena, E.T., and
794 Eliceiri, K.W. (2017). ImageJ2: ImageJ for the next generation of scientific image data.
795 Bmc Bioinformatics *18*.
796 44. Schindelin, J., Arganda-Carreras, I., Frise, E., Kaynig, V., Longair, M., Pietzsch, T.,
797 Preibisch, S., Rueden, C., Saalfeld, S., Schmid, B., et al. (2012). Fiji: an open-source
798 platform for biological-image analysis. Nature Methods *9*, 676-682.
799 45. Arganda-Carreras, I., Kaynig, V., Rueden, C., Schindelin, J., Cardona, A., and Seung,
800 H.S. (2016). Trainable_Segmentation: Release v3.1.2. (Zenodo).
801 46. Legland, D., Arganda-Carreras, I., and Andrey, P. (2016). MorphoLibJ: integrated
802 library and plugins for mathematical morphology with ImageJ. Bioinformatics *32*,
803 3532-3534.
804 47. Ohlsson, C., Henning, P., Nilsson, K.H., Wu, J.Y., Gustafsson, K.L., Sjogren, K.,
805 Tornqvist, A., Koskela, A., Zhang, F.P., Lagerquist, M.K., et al. (2018). Inducible Wnt16
806 inactivation: WNT16 regulates cortical bone thickness in adult mice. Journal of
807 Endocrinology *237*, 113-122.
808 48. Watson , C., J.,, Monstad-Rios , A., T,., Bhimani , R., M.,, Gistelinck , C., Willaert ,
809 A., Coucke , P., Hsu , Y., and Kwon, R., Y., (2019). Decoding G0 somatic mutants
810 through deep phenotyping and mosaic pattern analysis in the zebrafish skeleton.
811 BioRxiv, https://doi.org/10.1101/466185.
812 49. Schindeler, A., McDonald, M.M., Bokko, P., and Little, D.G. (2008). Bone remodeling
813 during fracture repair: The cellular picture. Seminars in Cell & Developmental Biology
814 *19*, 459-466.
815 50. Kim, Y.H., Cho, K.A., Lee, H.J., Park, M., Kim, H.S., Park, J.W., Woo, S.Y., and Ryu, K.H.
816 (2019). Identification of WNT16 as a Predictable Biomarker for Accelerated
817 Osteogenic Differentiation of Tonsil-Derived Mesenchymal Stem Cells In Vitro. Stem
818 Cells International *2019*.
819 51. Loi, F., Cordova, L.A., Pajarinen, J., Lin, T.H., Yao, Z.Y., and Goodman, S.B. (2016).
820 Inflammation, fracture and bone repair. Bone *86*, 119-130.
821 52. Claes, L., Recknagel, S., and Ignatius, A. (2012). Fracture healing under healthy and
822 inflammatory conditions. Nature Reviews Rheumatology *8*, 133-143.
823 53. Jung, Y.S., Lee, H.Y., Kim, S.D., Park, J.S., Kim, J.K., Suh, P.G., and Bae, Y.S. (2013).
824 Wnt5a stimulates chemotactic migration and chemokine production in human
825 neutrophils. Experimental and Molecular Medicine *45*.

bioRxiv preprint doi: https://doi.org/10.1101/2020.05.20.106328; this version posted May 21, 2020. The copyright holder for this preprint (which was not certified by peer review) is the author/funder, who has granted bioRxiv a license to display the preprint in perpetuity. It is made available under aCC-BY 4.0 International license.

826 54. Ohlsson, C., Nilsson, K.H., Henning, P., Wu, J.Y., Gustafsson, K.L., Poutanen, M.,
827 Lerner, U.H., and Moverare-Skrtic, S. (2018). WNT16 overexpression partly protects
828 against glucocorticoid-induced bone loss. American Journal of Physiology-
829 Endocrinology and Metabolism *314*, E597-E604.
830 55. Kobayashi, Y., Thirukonda, G.J., Nakamura, Y., Koide, M., Yamashita, T., Uehara, S.,
831 Kato, H., Udagawa, N., and Takahashi, N. (2015). Wnt16 regulates osteoclast
832 differentiation in conjunction with Wnt5a. Biochemical and Biophysical Research
833 Communications *463*, 1278-1283.
834 56. Kobayashi-Sun, J., Yamamori, S., Kondo, M., Kuroda, J., Ikegame, M., Suzuki, N.,
835 Kitamura, K., Hattori, A., Yamaguchi, M., and Kobayashi, I. (2020). Uptake of
836 osteoblast-derived extracellular vesicles promotes the differentiation of osteoclasts
837 in the zebrafish scale. Communications Biology *3*.
838 57. Gibon, E., Loi, F., Cordova, L.A., Pajarinen, J., Lin, T., Lu, L., Nabeshima, A., Yao, Z.,
839 and Goodman, S.B. (2016). Aging Affects Bone Marrow Macrophage Polarization:
840 Relevance to Bone Healing. Regenerative Engineering and Translational Medicine *2*,
841 98-104.
842 58. Logan, C.Y., and Nusse, R. (2004). The Wnt signaling pathway in development and
843 disease. Annual Review of Cell and Developmental Biology *20*, 781-810.
844 59. Zhong, N., Gersch, R.P., and Hadjiargyrou, M. (2006). Wnt signaling activation during
845 bone regeneration and the role of Dishevelled in chondrocyte proliferation and
846 differentiation. Bone *39*, 5-16.
847 60. Kahler, R.A., and Westendorf, J.J. (2003). Lymphoid enhancer factor-1 and beta-
848 catenin inhibit Runx2-dependent transcriptional activation of the osteocalcin
849 promoter. Journal of Biological Chemistry *278*, 11937-11944.
850 61. Schulte-Merker, S., and Stainier, D.Y.R. (2014). Out with the old, in with the new:
851 reassessing morpholino knockdowns in light of genome editing technology.
852 Development *141*, 3103-3104.
853 62. Alexander, K.A., Chang, M.K., Maylin, E.R., Kohler, T., Muller, R., Wu, A.C., Van
854 Rooijen, N., Sweet, M.J., Hume, D.A., Raggatt, L.J., et al. (2011). Osteal Macrophages
855 Promote In Vivo Intramembranous Bone Healing in a Mouse Tibial Injury Model.
856 Journal of Bone and Mineral Research *26*, 1517-1532.
857 63. Ferrero, G., Gomez, E., Iyer, S., Rovira, M., Miserocchi, M., Langenau, D.M., Bertrand,
858 J.Y., and Wittamer, V. (2020). The macrophage-expressed gene (mpeg) 1 identifies a
859 subpopulation of B cells in the adult zebrafish. Journal of Leukocyte Biology *107*,
860 431-443.
861 64. Marsell, R., and Einhorn, T.A. (2011). The biology of fracture healing. Injury-
862 International Journal of the Care of the Injured *42*, 551-555.
863

bioRxiv preprint doi: https://doi.org/10.1101/2020.05.20.106328; this version posted May 21, 2020. The copyright holder for this preprint (which was not certified by peer review) is the author/funder, who has granted bioRxiv a license to display the preprint in perpetuity. It is made available under aCC-BY 4.0 International license.

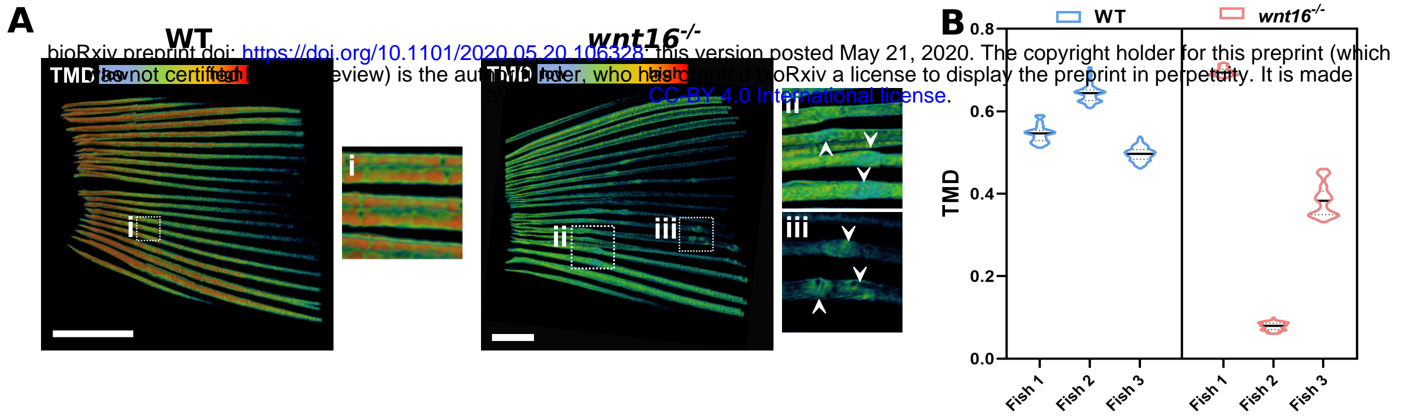

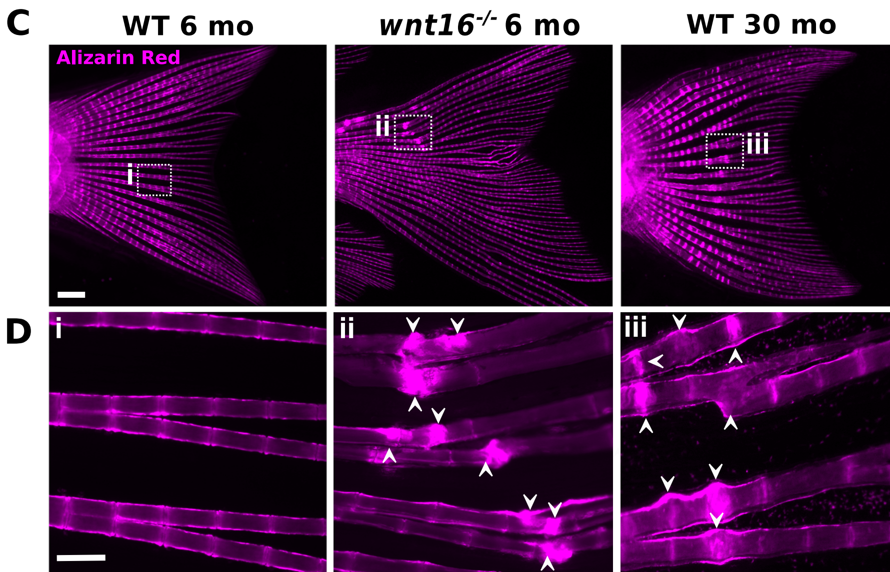

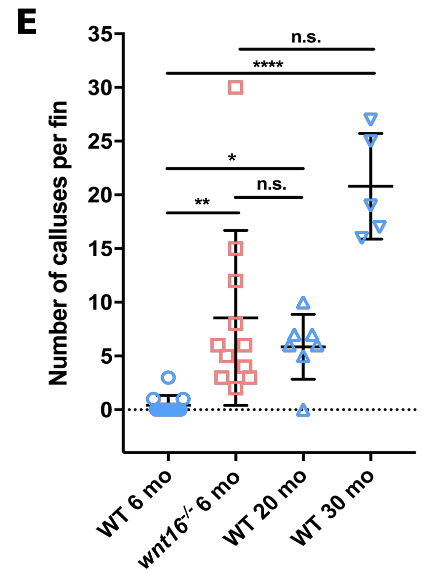

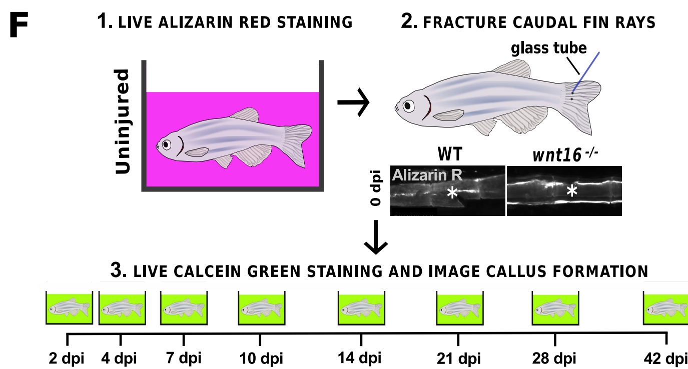

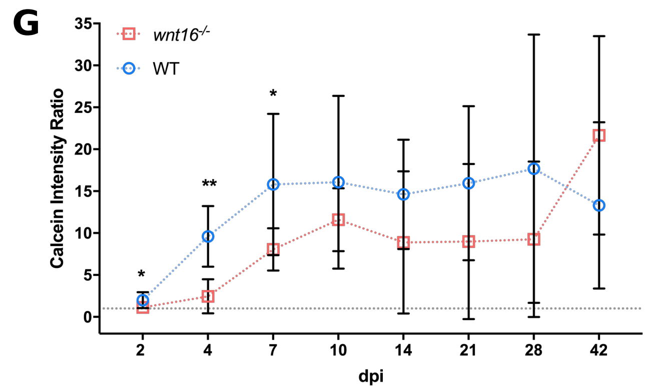

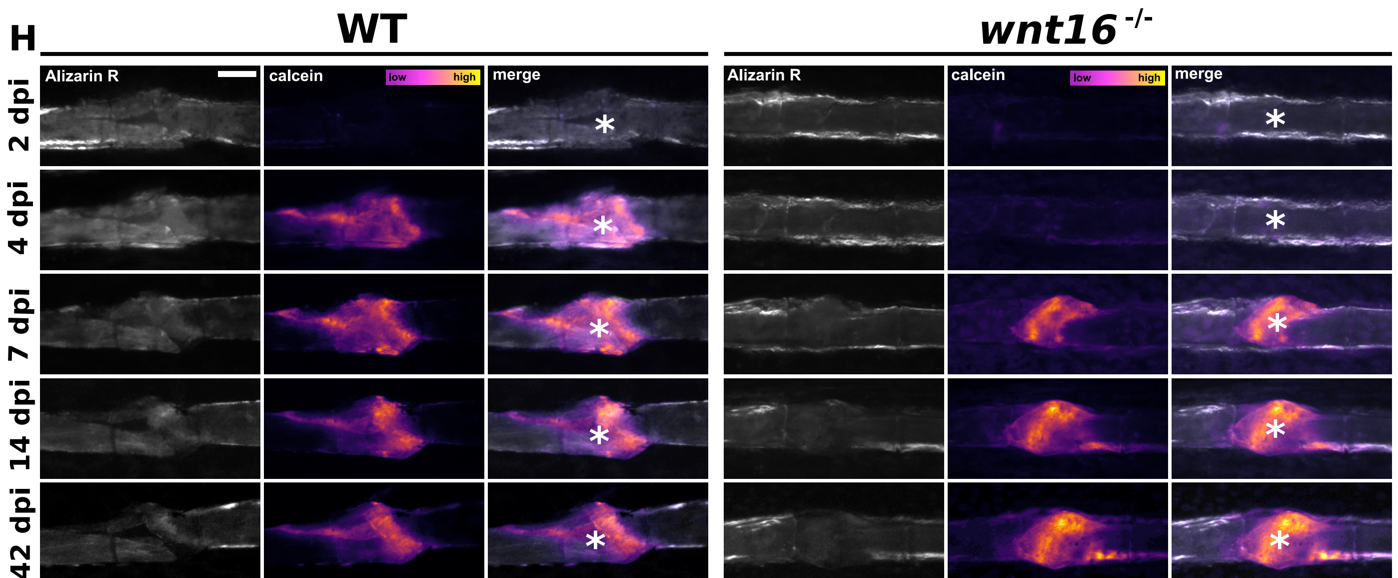

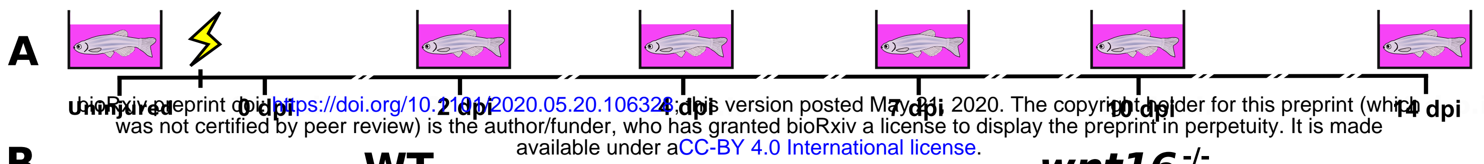

bioRxiv preprint doi: https://doi.org/10.1101/2020.05.20.106328; this version posted May 21, 2020. The copyright holder for this preprint (which was not certified by peer review) is the author/funder, who has granted bioRxiv a license to display the preprint in perpetuity. It is made available under aCC-BY 4.0 International license.

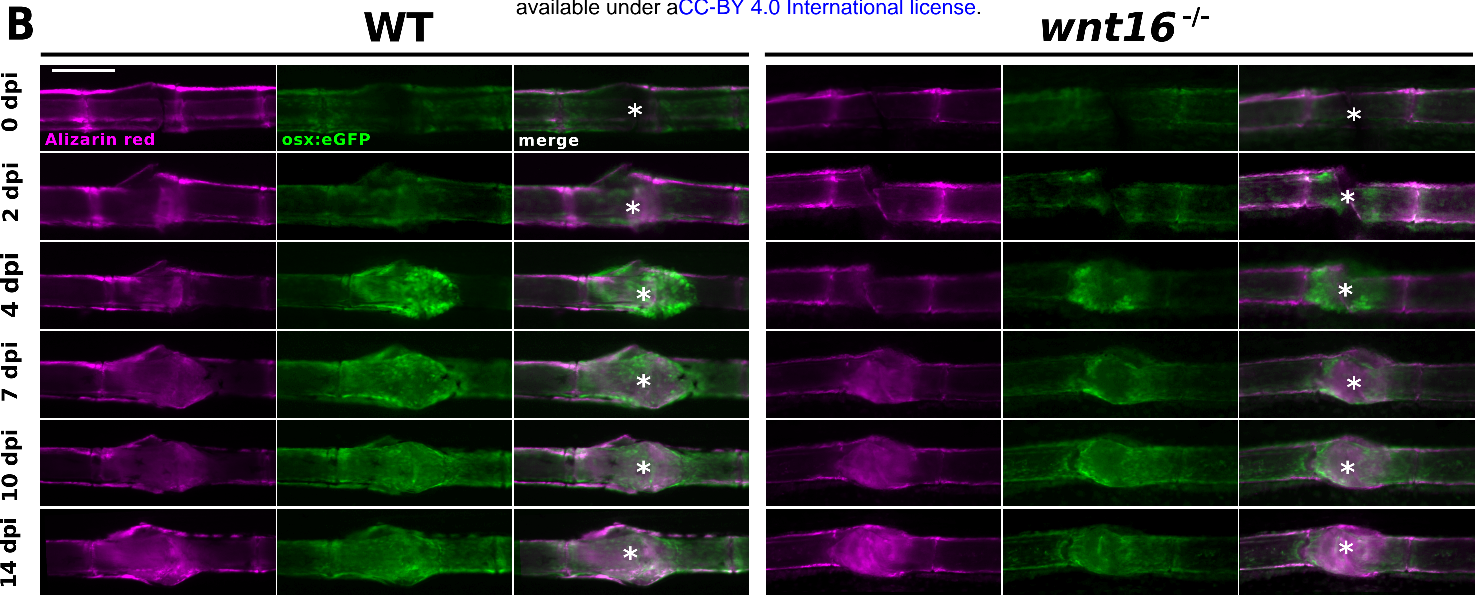

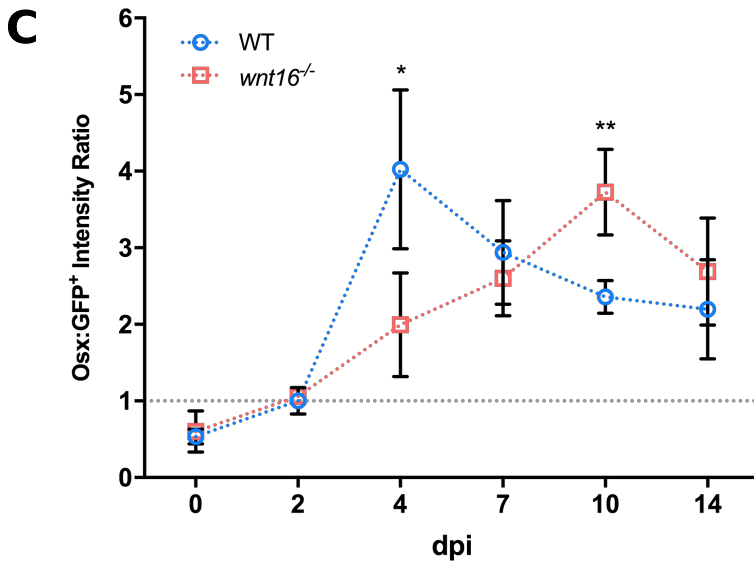

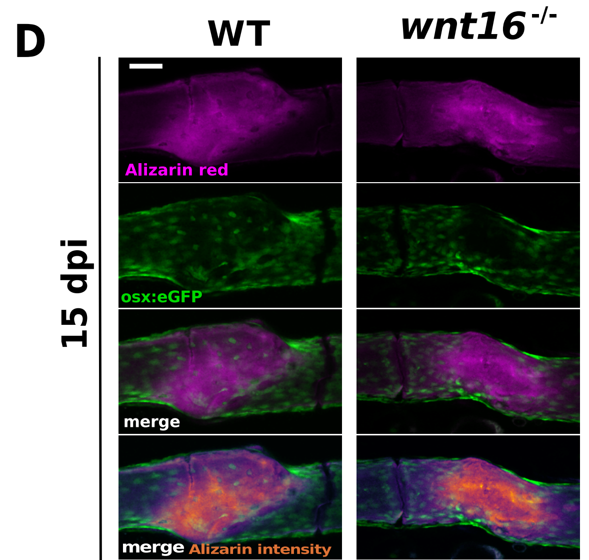

bioRxiv preprint doi: https://doi.org/10.1101/2020.05.20.106328; this version posted May 21, 2020. The copyright holder for this preprint (which was not certified by peer review) is the author/funder, who has granted bioRxiv a license to display the preprint in perpetuity. It is made available under aCC-BY 4.0 International license.

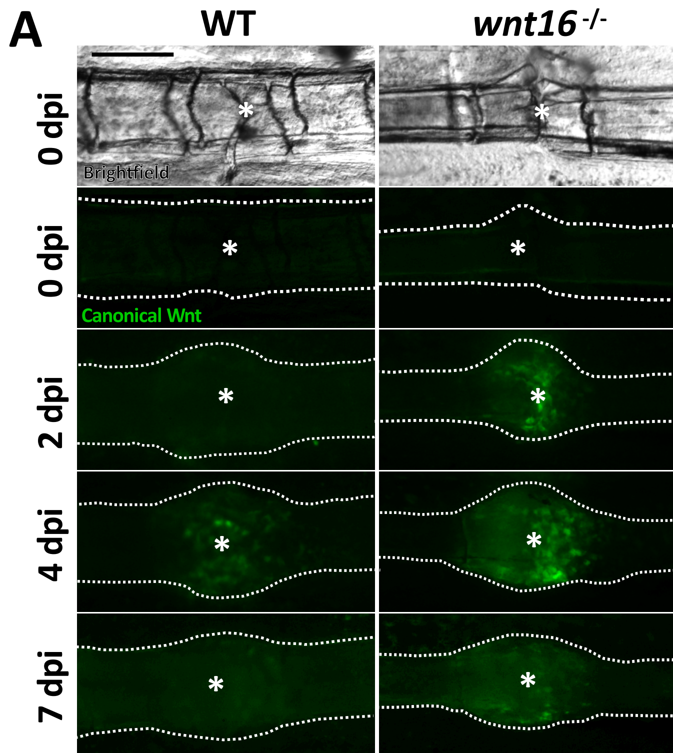

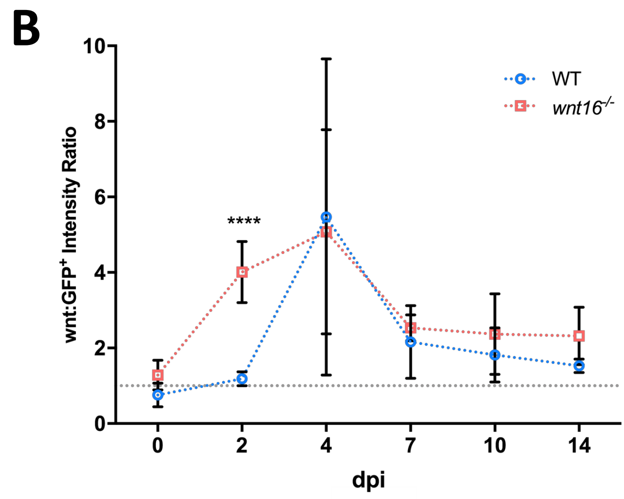

bioRxiv preprint doi: https://doi.org/10.1101/2020.05.20.106328; this version posted May 21, 2020. The copyright holder for this preprint (which was not certified by peer review) is the author/funder, who has granted bioRxiv a license to display the preprint in perpetuity. It is made available under aCC-BY 4.0 International license.

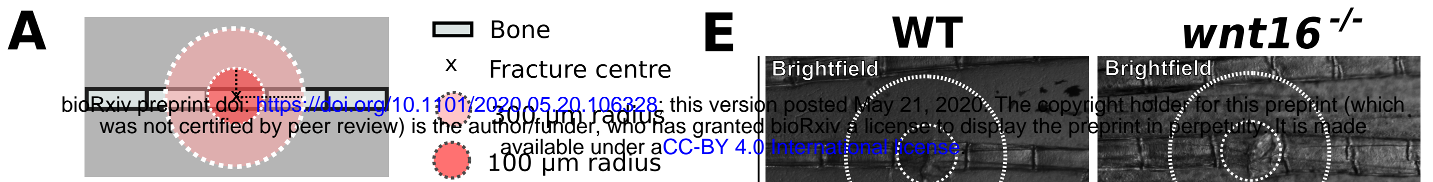

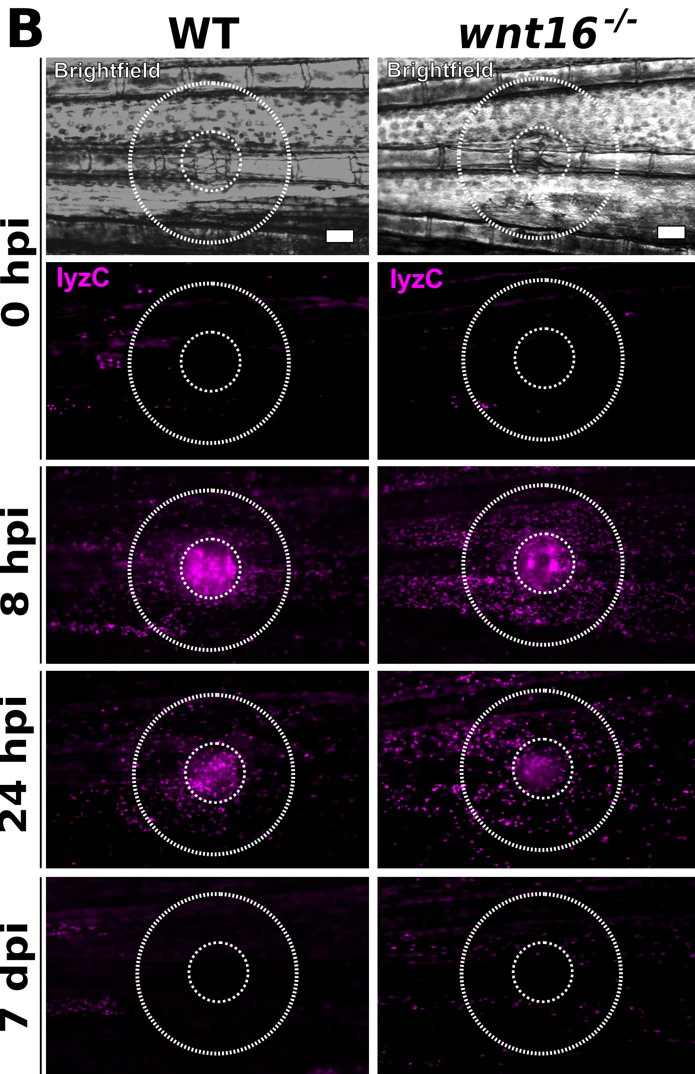

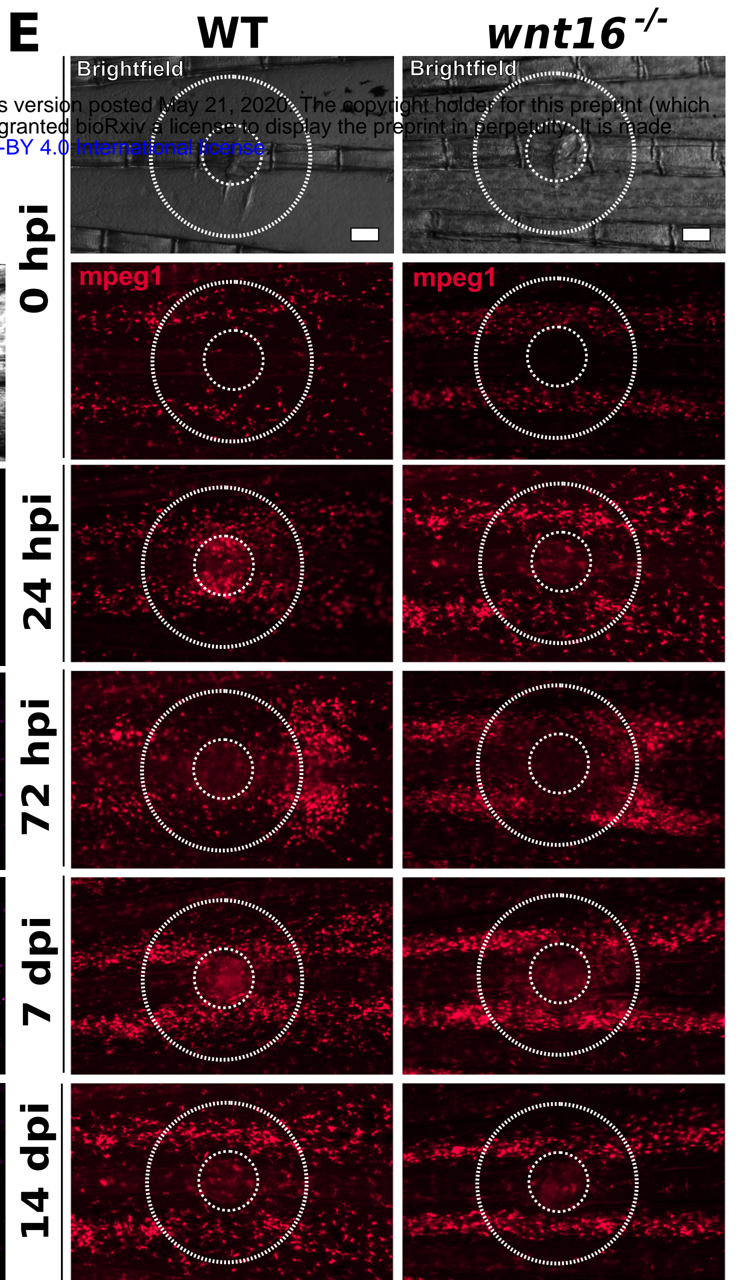

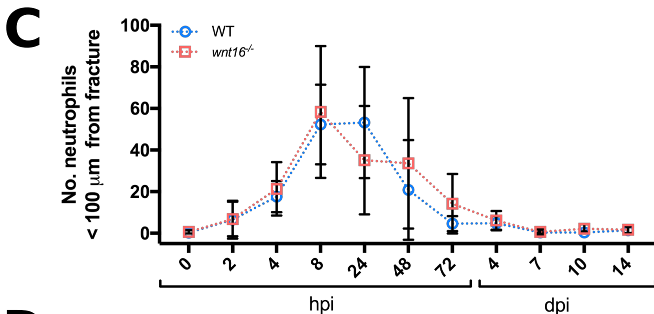

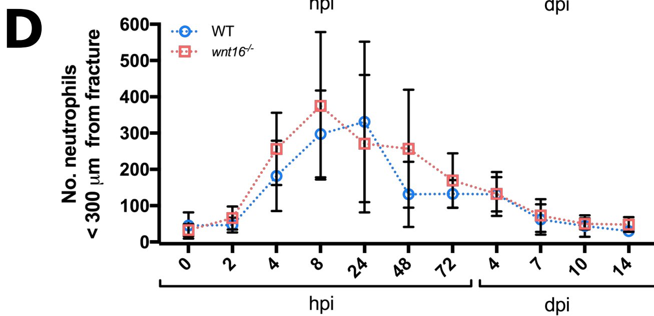

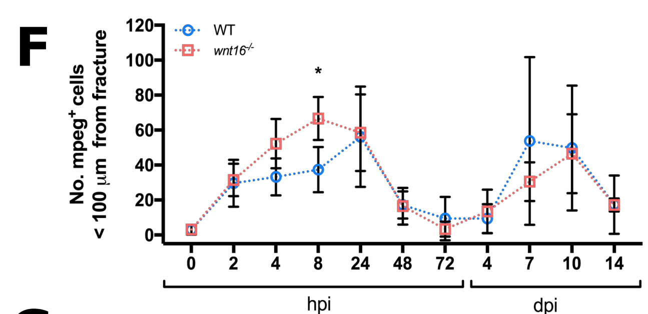

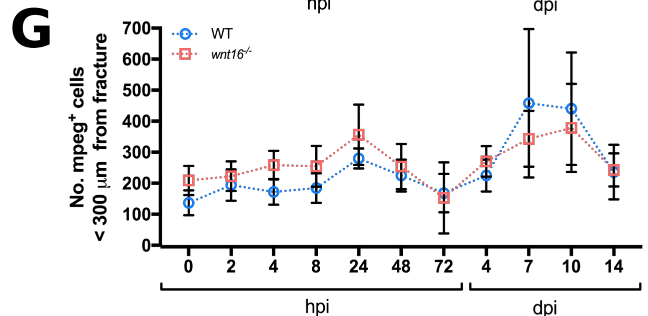

bioRxiv preprint doi: https://doi.org/10.1101/2020.05.20.106328; this version posted May 21, 2020. The copyright holder for this preprint (which was not certified by peer review) is the author/funder, who has granted bioRxiv a license to display the preprint in perpetuity. It is made available under aCC-BY 4.0 International license.